

First principles study of the crystal structure and dehydrogenation pathways of $\text{Li}_4\text{BN}_3\text{H}_{10}$

Donald J. Siegel and C. Wolverton

Physical and Environmental Sciences Department, Ford Motor Company, MD3083/RIC, Dearborn, MI 48121

V. Ozoliņš

Department of Materials Science and Engineering, University of California, Los Angeles, CA 90095

(Dated: July 23, 2021)

Using density functional theory we examine the crystal structure and the finite-temperature thermodynamics of formation and dehydrogenation for the new quaternary hydride $\text{Li}_4\text{BN}_3\text{H}_{10}$. Two recent studies based on X-ray and neutron diffraction have reported three bcc crystal structures for this phase. While these structures possess identical space groups and similar lattice constants, internal coordinate differences result in bond length discrepancies as large as 0.2 Å. Geometry optimization calculations on the experimental structures reveal that the apparent discrepancies are an artifact of X-ray interactions with strong bond polarization; the relaxed structures are essentially identical. Regarding reaction energetics, the present calculations predict that the formation reaction $3 \text{LiNH}_2 + \text{LiBH}_4 \rightarrow \text{Li}_4\text{BN}_3\text{H}_{10}$ is exothermic with enthalpy $\Delta H^{T=300\text{K}} = -11.8 \text{ kJ}/(\text{mol f.u.})$, consistent with reports of spontaneous $\text{Li}_4\text{BN}_3\text{H}_{10}$ formation in the literature. Calorimetry experiments have been reported for the dehydrogenation reaction, but have proven difficult to interpret. To help clarify the thermodynamics we evaluate the free energies of seventeen candidate dehydrogenation pathways over the temperature range $T = 0\text{--}1000 \text{ K}$. At temperatures where H_2 -release has been experimentally observed ($T \approx 520\text{--}630 \text{ K}$), the favored dehydrogenation reaction is $\text{Li}_4\text{BN}_3\text{H}_{10} \rightarrow \text{Li}_3\text{BN}_2 + \text{LiNH}_2 + 4\text{H}_2$, which is weakly endothermic [$\Delta H^{T=550\text{K}} = 12.8 \text{ kJ}/(\text{mol H}_2)$]. The small calculated ΔH is consistent with the unsuccessful attempts at re-hydriding reported in the literature, and suggests that the moderately high temperatures needed for H-desorption result from slow kinetics.

PACS numbers: 64.70.Hz, 65.40.-b, 71.15.Nc, 81.05.Zx

I. INTRODUCTION

Recent efforts to improve the efficiency and reduce the environmental impact of automobile transport have focused on hydrogen-based fuel cells (FC) and internal combustion engines (H_2ICE) as possible replacements for current technologies powered by fossil-fuels.¹ A significant obstacle to realizing this transition is the on-board storage of hydrogen at high gravimetric and volumetric densities.² To achieve the storage densities necessary for mobile applications, novel means for H-storage are necessary, and a set of targets have been established to guide the search for new storage systems.³ At present no known storage material or mechanism meets these targets.

One promising avenue for efficient storage of hydrogen is via solid state storage, such as in the form of complex- or metal-hydrides. Solid storage has the advantage of providing volumetric densities beyond what can be achieved with compressed H_2 gas or cryogenic liquid storage. However, all known hydrides suffer from one or more of the following limitations: low gravimetric densities, high H-desorption temperatures, or an inability to be easily re-hydrated. The search for new hydrides that overcome these limitations has attracted intense interest during the past 5 years.

Towards these ends, recent experiments by Pinkerton and co-workers^{4,5,6} and Aoki *et al.*^{7,8} on the H-storage properties of the quaternary Li-B-N-H system are noteworthy. By mixing lithium borohydride (LiBH_4) and lithium amide (LiNH_2), both groups have reported the formation of a new hydride phase, which when heated above $\sim 520 \text{ K}$ released approximately 10 wt.% hydrogen. While the reported desorption temperature is somewhat too high, and reversibility has not yet been demonstrated, improvement in these areas may be

possible (and has been partially demonstrated⁶) through the addition of catalytic dopants^{6,9} or via novel synthetic routes,¹⁰ suggesting that further study of this system is warranted.

The composition of the new Li-B-N-H phase was preliminarily identified⁴ as “ $\text{Li}_3\text{BN}_2\text{H}_8$,” but subsequent experiments based on single crystal X-ray diffraction,¹¹ and, synchrotron X-ray and neutron powder diffraction,¹² identified its true stoichiometry as $\text{Li}_4\text{BN}_3\text{H}_{10}$. Combined, these diffraction experiments identified three similar crystal structures, all sharing the bcc space group $I2_13$ with lattice constant $a = 10.66\text{--}10.68 \text{ Å}$, but with somewhat different internal coordinates. The discrepancy in atomic positions results in N-H bond lengths that differ between structures by as much as 0.2 Å, with smaller N-H lengths reported for the X-ray structures. It has been suggested that the discrepancy may be an artifact of X-ray interactions with strongly polarized electron clouds along the N-H bond direction.¹¹

A careful characterization of a hydride’s crystal structure is desirable because it enables an independent, *ab initio* assessment of the thermodynamics of hydrogen desorption/absorption reactions. Such an assessment is of value because it can clarify the thermodynamics when calorimetry measurements yield ambiguous results, such as in situations where multiple reactions occur simultaneously (see below). A key thermodynamic property which determines the suitability of a hydride for H-storage applications is the strength of the hydrogen-host bond. The bond strength is quantified via the change in enthalpy (ΔH) occurring during hydrogen uptake/release. In mobile FC applications, for example, it is desirable that the desorption reaction be *endothermic* ($\Delta H > 0$) with $\Delta H \approx 20\text{--}50 \text{ kJ}/(\text{mol H}_2)$. Neglecting kinetics, an enthalpy in this range would allow for H-desorption at temper-

atures compatible with the waste heat from a FC, and permit on-board recharging under reasonable H₂ pressure.

Unfortunately, calorimetric measurements of H-desorption in Li₄BN₃H₁₀ have been difficult to interpret. (See Refs. 6 and 8, and the supplementary information accompanying Ref. 4.) Because Li₄BN₃H₁₀ melts at ~460 K, approximately 60 degrees below the onset of H-desorption, hydrogen gas evolves from the liquid state.⁴ Concurrent with H₂ release is the formation of a solid reaction product, generally involving one or more polymorphs of Li₃BN₂ along with other unidentified phases,^{4,7,8} and desorption of 2-3 mol % ammonia.⁴ Measurements based on differential scanning calorimetry (DSC)^{4,6} and differential thermal analysis (DTA)⁸ suggest that the *net* heat flow during dehydriding is exothermic ($\Delta H < 0$). However, it is unclear what fraction of the total thermal profile arises from the exothermic latent heat of Li₃BN₂ solidification,⁸ and furthermore how H₂ and NH₃ release impacts the calorimeter response.⁴ Consequently, it has not been possible to unambiguously assess the endo- or exothermic nature of H-desorption alone. Neglecting kinetic effects, the fact that it has proven very difficult⁴ to re-hydride Li₄BN₃H₁₀ suggests desorption is weakly endothermic, or exothermic. Regarding Li₄BN₃H₁₀ formation, several studies^{4,8,12} have reported the spontaneous formation of Li₄BN₃H₁₀ after mixing LiBH₄ with LiNH₂, even at temperatures as low as room temperature, suggesting that the formation reaction is exothermic.⁴

In light of the discrepancy noted above regarding the crystal structure of Li₄BN₃H₁₀, and the additional ambiguity surrounding its dehydrogenation thermodynamics, we employ density functional theory (DFT)^{13,14} calculations in an attempt to clarify these issues. First, we determine the ground state crystal structure by performing separate geometry optimization calculations on each of the experimentally proposed crystal structures. We find that the relaxed structures are essentially identical, and have N-H bond lengths that are consistent with the structure based on neutron diffraction,¹² thus confirming the conjecture¹¹ that the anomalously short N-H bond lengths observed in Ref. 11 are an artifact of X-ray measurements. Second, we evaluate the finite-temperature reaction enthalpies and free energies for the formation and dehydrogenation of Li₄BN₃H₁₀. Li₄BN₃H₁₀ formation (with respect to LiNH₂ and LiBH₄) is found to be exothermic, in agreement with experimental reports of spontaneous Li₄BN₃H₁₀ formation in the literature.^{4,7,12} For H₂-desorption we explore the thermodynamics of seventeen candidate reactions over the temperature range $T = 0$ –1000 K, as there appears to be some uncertainty in determining the reaction products experimentally.^{4,7} At temperatures where desorption has been reported⁴ ($T \approx 520$ –630 K), the favored reaction is predicted to be Li₄BN₃H₁₀ \rightarrow Li₃BN₂ + LiNH₂ + 4 H₂, which is weakly endothermic. Moreover, the calculated free energies suggest Li₄BN₃H₁₀ is a metastable phase that should decompose via one of three temperature-dependent pathways.

II. METHODOLOGY

First-principles calculations were performed using a planewave method based on the PW91 generalized gradient approximation¹⁵ to density functional theory^{13,14} (VASP).¹⁶ The core-valence electron interaction was treated using Blöchl’s projector augmented wave (PAW) method,^{17,18} and k-point sampling was performed on a dense Monkhorst-Pack¹⁹ grid with an energy convergence of better than 1 meV per supercell. (In the case of Li₄BN₃H₁₀, a $2 \times 2 \times 2$ grid was sufficient to achieve this level of precision.) Electronic occupancies were determined via a gaussian smearing algorithm with a 0.1 eV smearing width. For high-precision calculation of static zero Kelvin (omitting zero point vibrational effects) electronic energies and crystal structures we used the so-called “hard” VASP PAW potentials⁵¹ with a planewave cutoff of 875 eV, and a geometry relaxation tolerance of better than 0.02 eV/Å. Internal atomic positions and external cell shape/volume were optimized simultaneously.

Finite-temperature thermodynamics were evaluated within the harmonic approximation.^{20,21} Vibrational frequencies (ω_i) were extracted by diagonalizing a dynamical matrix whose elements were determined via the so-called direct method:²² the forces generated by series of symmetry inequivalent atomic displacements about the equilibrium geometry (± 0.02 Å, ± 0.04 Å) were fit to cubic splines in order to extract the force constants. Because large supercells are desirable to minimize finite-size effects, and with the exception of the molecular species (H₂, N₂, NH₃) where the number of atoms per supercell is small, the dynamical matrix calculations on the solid-state phases were performed using a softer set of PAW potentials⁵² and planewave cutoff energies ranging from 400–500 eV.⁵³ A comparison of calculated structural parameters and formation energies with existing experimental and theoretical data is presented in the following section.

Once the normal-mode frequencies have been determined, finite-temperature energetics can be obtained by enthalpic (H_{vib}) and entropic (S_{vib}) additions to the static electronic energies. Within the harmonic approximation these contributions are given by:²⁰

$$H_{\text{vib}}(T) = \sum_i \frac{1}{2} \hbar \omega_i + \hbar \omega_i \left[\exp\left(\frac{\hbar \omega_i}{k_B T}\right) - 1 \right]^{-1} \quad (1)$$

$$S_{\text{vib}}(T) = k_B \sum_i \frac{\hbar \omega_i / k_B T}{\exp\left(\frac{\hbar \omega_i}{k_B T}\right) - 1} - \ln \left[1 - \exp\left(\frac{-\hbar \omega_i}{k_B T}\right) \right], \quad (2)$$

where the sums run over vibrational frequencies ($3N - 3$ frequencies for solids and non-linear molecules, $3N - 5$ frequencies for linear molecules), k_B is the Boltzmann factor, and T is the absolute temperature. For the linear (non-linear) molecules an additional $\frac{7}{2} k_B T$ ($4 k_B T$) term is added to Eq. 1 to account for translational, rotational, and pV degrees of freedom. The zero point energy (ZPE) can be recovered from Eq. 1 in the limit $H_{\text{vib}}(T = 0)$. The enthalpy and free energy

of a phase can therefore be expressed as:

$$H(T) = E + H_{\text{vib}}(T) \quad (3)$$

$$G(T) = H(T) - S(T)T, \quad (4)$$

where E is the static electronic energy of the crystal/molecule in its ground-state geometry and S represents either the standard tabulated²³ entropy of a given molecular species in the gas phase at $p = 1$ bar [$S_0^{T=300\text{K}} = 130.858$ (H₂), 191.789 (N₂), and 192.995 J K⁻¹ mol⁻¹ (NH₃)], or the vibrational entropy S_{vib} of a solid state phase.

III. CRYSTAL STRUCTURE

The crystal structure of Li₄BN₃H₁₀ has been studied by two groups.^{11,12} Filinchuk and co-workers¹¹ used single-crystal X-ray diffraction to identify the structures of the two largest crystal domains obtained after remelting a 2:1 mixture of LiNH₂ and LiBH₄. Both domains exhibited a bcc structure (space group $I2_13$) with lattice constants of 10.67-10.68 Å. Chater *et al.*¹² used a combination of high-resolution synchrotron X-ray and neutron diffraction to examine powder samples prepared from a wide range of LiNH₂:LiBH₄ compositions. They determined that although the most likely stoichiometric composition was 3:1, the Li₄BN₃H₁₀ structure was able to accommodate a wide range of stoichiometries. Their best-fit crystal structure had external cell parameters similar to those reported in Ref. 11: bcc (space group $I2_13$) with $a = 10.66$ Å. Despite the good agreement in external geometries, the structures obtained by these two studies differ markedly in their internal coordinates. Most notably, the single-crystal X-ray diffraction study¹¹ found anomalously short N-H bond lengths of 0.83-0.86 Å, while neutron scattering¹² gave lengths of 0.98-1.04 Å.

The external cell parameters obtained upon relaxing each of the three Li₄BN₃H₁₀ experimental structures (as well as the structures of the other phases used in our subsequent discussion of reaction thermodynamics) are summarized in Table I. The resulting structures are bcc and share the same lattice constant, $a = 10.60$ Å, in good agreement with both diffraction studies.

For each of the three relaxed structures, Table II compares the calculated internal atomic coordinates with the corresponding experimental values. We note first that the average absolute deviation (δ) between theory and experiment is smallest for the neutron structure,¹² $\delta = 3.6 \times 10^{-3}$, whereas for the X-ray structure¹¹ $\delta = 4.4 \times 10^{-3}$ and $\delta = 4.2 \times 10^{-3}$ for domains 1 and 2, respectively. The largest discrepancy between theory and experiment is in the positions of the N-bonded hydrogen atoms, H1 & H2, in the X-ray structure. (Note that the labeling convention for hydrogens is different in the neutron structure: there H1 & H2 refer to B-bonded hydrogens.) Secondly, while there appear to be large differences in the internal coordinates measured by Refs. 11 and 12 (Table II), after relaxation these three structures may be mapped onto one another via a series of rigid body rotations and translations. We conclude that all three experimental structures relax to essentially the same structure.

TABLE I: Calculated structural parameters compared with experimental data. Bond lengths (d) and crystal lattice constants (a , b , c) are given in Å, bond angles (\angle) and angles between lattice vectors (α , β) are listed in degrees. Space group information for the solid phases is listed in parentheses.

System	Parameter	Calculated	Experiment
H ₂	$d(\text{H-H})$	0.749	0.741 ²⁴
N ₂	$d(\text{N-N})$	1.101	1.098 ²⁴
NH ₃	$d(\text{N-H})$	1.021	1.012 ²⁴
	$\angle(\text{H-N-H})$	106.4	106.7 ²⁴
α -B ($R\bar{3}m$)	a	5.05	5.06 ²⁵
	α	58.1	58.1 ²⁵
BN ($F\bar{4}3m$)	a	3.62	3.62 ²⁶
Li ($Im\bar{3}m$)	a	3.44	3.51 ²⁷
LiH ($Fm\bar{3}m$)	a	4.01	4.07 ²⁸
Li ₃ N ($P\bar{3}m1$)	a	3.64	3.61 ^a
	c	3.88	3.85 ^a
LiNH ₂ ($I\bar{4}$)	a	5.02	5.04 ²⁹
	c	10.28	10.28 ²⁹
Li ₂ NH ($Pnma$)	a	7.75	7.73 ^b
	b	3.61	3.60 ^b
	c	4.88	4.87 ^b
α -Li ₃ BN ₂ (PA_2/mnm)	a	4.67	4.64 ^{30,31}
	c	5.22	5.26 ^{30,31}
β -Li ₃ BN ₂ ($P2_1/c$)	a	5.15	5.15 ³²
	b	7.08	7.08 ³²
	c	6.77	6.79 ³²
	β	112.7	113.0 ³²
Li ₃ BN ₂ ($I4_1/amd$)	a	6.63	6.60 ³³
	c	10.35	10.35 ³³
LiBH ₄ ($Pnma$)	a	7.25	7.18 ³⁴
	b	4.38	4.44 ³⁴
	c	6.63	6.80 ³⁴
Li ₄ BN ₃ H ₁₀ ($I2_13$)	a	10.60	10.67-10.68 ¹¹ 10.66 ¹²

^aTheoretically predicted structure from Ref. 35. In agreement with Ref. 35, we find the room-temperature experimental $P6/mmm$ structure to be unstable at low temperature, with a weak soft mode of 66i cm⁻¹.

^bTheoretically predicted structure from Ref. 36.

A comparison of calculated bond lengths, bond angles, and intermolecular distances is given in Table III. Overall, the relaxed structures agree best with the *intramolecular* lengths (i.e., within an NH₂ or BH₄ fragment) determined using neutron diffraction; conversely, the *intermolecular* distances from X-ray are closest to those in the relaxed theoretical structures. As for the intramolecular structure, as noted above, the major discrepancy between the experimental structures lies in the two N-H bond lengths, $d(\text{N-H})$, in the NH₂ fragment. The calculated length of 1.027 Å is in better agreement with the longer bond lengths predicted by neutron diffraction of 0.983 and 1.042 Å. Similarly, the X-ray data also underestimates B-H bond lengths in the BH₄ units relative to our DFT calculations and neutron data. Calculated bond angles agree best with those from the neutron structure.

TABLE II: Calculated relaxed internal atomic positions of $\text{Li}_4\text{BN}_3\text{H}_{10}$ compared with experimental measurements from Refs. 11,12.

Atom	Calculated			Experiment			
	x	y	z	x	y	z	
N	0.117	0.362	0.402	0.115	0.359	0.405	Domain 1, Ref. 11
B	0.113	0.113	0.113	0.114	0.114	0.114	
Li1	0.281	0.000	0.250	0.287	0.000	0.250	
Li2	0.519	0.000	0.250	0.524	0.000	0.250	
Li3	0.484	0.484	0.484	0.483	0.483	0.483	
H1	0.195	0.306	0.393	0.175	0.310	0.397	
H2	0.118	0.415	0.321	0.115	0.405	0.339	
H3	0.003	0.118	0.147	0.012	0.119	0.146	
H4	0.180	0.180	0.180	0.172	0.172	0.172	
N	0.117	0.361	0.402	0.115	0.359	0.405	Domain 2, Ref. 11
B	0.113	0.113	0.113	0.114	0.114	0.114	
Li1	0.281	0.000	0.250	0.286	0.000	0.250	
Li2	0.519	0.000	0.250	0.523	0.000	0.250	
Li3	0.484	0.484	0.484	0.484	0.484	0.484	
H1	0.195	0.305	0.394	0.176	0.310	0.399	
H2	0.118	0.415	0.321	0.114	0.402	0.338	
H3	0.003	0.117	0.148	0.015	0.116	0.149	
H4	0.180	0.180	0.180	0.174	0.174	0.174	
N	-0.152	0.112	0.367	-0.156	0.110	0.367	Ref. 12
B	0.137	0.137	0.137	0.135	0.135	0.135	
Li1	0.250	-0.030	0.000	0.250	-0.043	0.000	
Li2	-0.268	0.000	0.250	-0.262	0.000	0.250	
Li3	0.266	0.266	0.266	0.272	0.272	0.272	
H1	0.071	0.071	0.071	0.072	0.072	0.072	
H2	0.103	0.133	0.247	0.097	0.136	0.248	
H3	-0.143	0.055	0.445	-0.153	0.053	0.439	
H4	-0.071	0.165	0.368	-0.077	0.167	0.377	

TABLE III: Comparison of calculated atomic distances and angles with values determined from single-crystal X-ray diffraction (Ref. 11) and synchrotron X-ray and neutron powder diffraction (Ref. 12). Lengths (d) are given in Å, angles (\angle) are in degrees.

Parameter	Ref. 11, domain 1		Ref. 11, domain 2		Ref. 12	
	Calculated	Experiment	Calculated	Experiment	Calculated	Experiment
Intramolecular Values						
$d(\text{N-H})$ (i)	1.027	0.83(2)	1.027	0.84(2)	1.027	0.983
$d(\text{N-H})$ (ii)	1.027	0.859	1.026	0.852	1.027	1.042
$d(\text{B-H})$ (i)	1.223	1.08(3)	1.225	1.11(3)	1.224	1.169
$d(\text{B-H})$ (ii) $\times 3$	1.225	1.137	1.225	1.121	1.223	1.270
$\angle(\text{H-N-H})$	103.5	106.2	103.5	105.9	103.5	104.9
$\angle(\text{H-B-H})\times 3$ (i)	108.0	108.9	107.9	109.2	107.9	107.6
$\angle(\text{H-B-H})\times 3$ (ii)	110.9	110.1	111.0	109.8	111.0	111.3
Intermolecular Values						
$d(\text{N-Li})$ (i)	2.071	2.069	2.069	2.068	2.070	2.033
$d(\text{N-Li})$ (ii)	2.116	2.115	2.111	2.113	2.110	2.053
$d(\text{N-Li})$ (iii)	2.138	2.117	2.138	2.119	2.142	2.094
$d(\text{N-Li})$ (iv)	2.164	2.157	2.164	2.157	2.169	2.209
$d(\text{B-Li})$ (i)	2.371	2.410	2.375	2.406	2.368	2.527
$d(\text{B-Li})$ (ii) $\times 3$	2.595	2.651	2.592	2.642	2.589	2.681

IV. REACTION ENERGETICS

In order to examine the finite-temperature thermodynamics of reactions involving $\text{Li}_4\text{BN}_3\text{H}_{10}$, it was first necessary to calculate the ground-state structures of the phases that participate in those reactions. A summary of the compounds used, their

crystal structures, and a comparison of the calculated structures to experimental data is presented in Table I. In general the agreement between experiment and theory is very good.

Some of the compounds listed in Table I are known to have several polymorphs. For example, at least three polymorphs have been reported for Li_3BN_2 ,^{31,32,37,38} including low-temperature tetragonal (α),³¹ high-temperature mon-

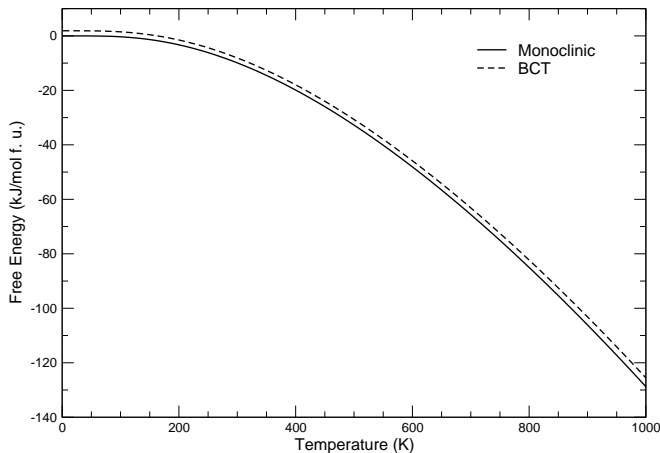


FIG. 1: Calculated Gibbs free energies (in kJ/mol f.u.) of monoclinic (β) and body-centered tetragonal (BCT) Li_3BN_2 as a function of temperature. The energy zero is set to the static 0 K energy of $\beta\text{-Li}_3\text{BN}_2$.

oclinic (β),³² and high-pressure body-centered tetragonal (bct)^{33,37,38} phases. All three of these phases have been observed as dehydrogenation products for $\text{Li}_4\text{BN}_3\text{H}_{10}$,^{4,8} and we have performed calculations on each phase to determine its relative stability as a function of temperature. The $\beta\text{-Li}_3\text{BN}_2$ phase was found to have the lowest zero-Kelvin static energy, ≈ 2 kJ/(mol f.u.) lower than that of either the bct or α phases. The latter two phases are degenerate in energy to within 0.1 kJ/(mol f.u.). Our zero-Kelvin energetics and structures agree well with recent calculations reported by Pinkerton and Herbst.³³

Vibrational contributions to the energies of each Li_3BN_2 polymorph were evaluated within the harmonic approximation. For $\alpha\text{-Li}_3\text{BN}_2$ a careful evaluation of the vibrational spectra yielded doubly-degenerate imaginary modes at $81i$ cm^{-1} , indicating that this phase is unstable at low temperatures. A search for alternative low-energy $\alpha\text{-Li}_3\text{BN}_2$ structures was performed using molecular dynamics (md) on an enlarged ($2 \times 2 \times 2$) $\alpha\text{-Li}_3\text{BN}_2$ supercell at $T = 423$ K for 10 ps. At 1 ps intervals the current md configuration was stored, relaxed, and the symmetry of the resulting optimized structure was determined. Four unique crystal structures were identified, with space groups (numbers): $P2_12_12_1$ (19), $Pccn$ (56), $Pmnm$ (59), and $Pnma$ (62). These structures were then relaxed within their symmetry constraints, and were found to have energies ~ 1 kJ/(mol f.u.) lower than the original $\alpha\text{-Li}_3\text{BN}_2$ structure [which is still 1 kJ/(mol f.u.) higher in energy than $\beta\text{-Li}_3\text{BN}_2$]. In light of these results we suggest that the crystal structure of $\alpha\text{-Li}_3\text{BN}_2$ be experimentally reassessed, and we exclude this phase from our evaluation of $\text{Li}_4\text{BN}_3\text{H}_{10}$ dehydrogenation reactions. Further information regarding our proposed structure of $\alpha\text{-Li}_3\text{BN}_2$ can be found elsewhere.³⁹

Unlike $\alpha\text{-Li}_3\text{BN}_2$, no imaginary modes were observed in the vibrational spectra of β or bct Li_3BN_2 . Using Eqs. 1-2, Fig. 1 plots the Gibbs free energies (Eq. 4) of these phases as a function of temperature. Due to their similar vibrational

TABLE IV: Calculated vibrational contributions (at $T = 300\text{K}$) to the free energies of phases used in this study. ZPE refers to the zero point energy, given by $H_{\text{vib}}(T = 0)$ (Eq. 1); $E_{\text{vib}} = H_{\text{vib}} - \text{ZPE}$ (omitting the $k_B T$ molecular terms); S_{vib} is the vibrational entropy, Eq. 2. Units are kJ mol^{-1} for ZPE and E_{vib} , and $\text{J mol}^{-1} \text{K}^{-1}$ for S_{vib} .

System	ZPE	ZPE other	$E_{\text{vib}}^{T=300\text{K}}$	$S_{\text{vib}}^{T=300\text{K}}$
H_2	25.7	25.7 ⁴⁰ , 26.1 ⁴¹ , 26.3 ⁴²	≈ 0	≈ 0
N_2	14.0	14.4 ⁴²	≈ 0	≈ 0
NH_3	87.8	89.7 ⁴³	0.1	0.4
Li	3.9	3.9 ⁴¹	4.3	27.7
B	12.5	12.2 ⁴¹	1.1	5.3
BN	29.9	30.9 ⁴⁴		
LiH	21.7	21.4, ⁴¹ 21.8 ³⁶	3.5	17.7
Li_3N	28.0	28.6 ³⁵		
LiNH_2	69.0	69.1, ³⁵ 69.5, ³⁶ 69.8 ⁴²	8.9	51.6
Li_2NH	46.7	46.7 ⁴² , 47.1 ³⁶	9.6	52.9
LiBH_4	107.1	103.0, ⁴¹ 106.5, ⁴⁰ 108.1 ⁴⁵	10.8	63.6
Li_3BN_2	52.2		15.3	83.8
$\text{Li}_4\text{BN}_3\text{H}_{10}$	314.4		37.0	213.4

contributions (Table IV), the free energies of the β and bct phases exhibit nearly identical temperature dependence. Consequently, the small ~ 2 kJ/(mol f.u.) difference in static energies noted above is sufficient to favor the monoclinic β phase as the ground state structure, and the bct- β energy difference remains roughly constant for $T < 1000$ K. Based on the vibrational instability observed in $\alpha\text{-Li}_3\text{BN}_2$, and the higher free energy of bct Li_3BN_2 (relative to $\beta\text{-Li}_3\text{BN}_2$), our subsequent thermodynamic analyses are performed assuming Li_3BN_2 resides in the the low-energy β structure.

The zero-point, enthalpic, and entropic contributions to the free energy of the various phases are summarized in Table IV. As a further test of our computational methodology, there we also compare our calculated ZPE to other values reported in the literature, and find good agreement. With the exception of Li, vibrational effects are found to contribute substantially to the free energies of these systems. For example, in $\text{Li}_4\text{BN}_3\text{H}_{10}$ the ZPE exceeds 300 kJ/mol.

A comparison of formation energies for the compounds used in this study (relative to the elements in their standard states) is presented in Table V. Three reports^{33,41,42} based on DFT calculations have also recently evaluated formation energies for some of these compounds, and the present calculations are in good agreement with their findings. Furthermore, the agreement with experimental enthalpies is reasonable (generally on the order of 10%), which is representative of the accuracy obtained via density functional methods for reactions involving molecular species.⁴⁷ As expected, the largest percentage discrepancy is for the ammonia molecule.⁵⁴ Two general trends in the data are evident: (i) With the exception of ammonia, the DFT enthalpies ($\Delta H^{T=300\text{K}}$) are more positive than the experimental values, and (ii) the inclusion of dynamical contributions ($\Delta E \rightarrow \Delta H^{T=300\text{K}}$) results in more

TABLE V: Comparison of calculated formation energies (with respect to the elements, in kJ/mol f.u.) with existing experimental and theoretical data. ΔE refers to differences in static 0 K energies, formation enthalpies (ΔH) and free energies (ΔG) are based on Eqns. 3 and 4, respectively. Experimental data is from Refs. 23 and 46, theoretical data is from a set of recent DFT calculations (Refs. 33,41,42).

System	ΔE	$\Delta H^{T=300K}$	$\Delta G^{T=300K}$
NH ₃	-98.0	-63.2 -45.9 ²³	-33.6 -16.2 ²³
BN	-233.8	-227.4 -250.9 ²³	-198.9 -224.9 ²³
LiH	-83.6 -81 ⁴¹ -83.9 ⁴²	-83.8 -90.6 ²³ -84.6 ⁴²	-61.2 -68.3 ²³
Li ₃ N	-148.7	-145.9 -164.6 ²³	-109.8 -128.4 ²³
LiNH ₂	-196.6 -196.5 ⁴²	-172.6 -176 ⁴⁶ -173.1 ⁴²	-111.7
Li ₂ NH	-196.0 -194.0 ⁴²	-184.5 -222 ⁴⁶ -184.1 ⁴²	-135.3
LiBH ₄	-205.9 -194 ⁴¹	-178.6 -190.5 ²³	-109.2 -124.3 ²³
Li ₃ BN ₂	-497.4 -497 ³³	-490.6	-433.6

positive formation energies.

Using the energetic contributions from Table IV, in Table VI we evaluate the thermodynamics for two Li₄BN₃H₁₀ formation reactions. Reaction (a) considers formation from the elemental phases in their standard states, and reaction (b) corresponds to the synthesis route employed in the literature^{4,7,12} involving a mixture of LiNH₂ and LiBH₄. (We consider only the stoichiometric¹² 3:1 ratio of LiNH₂ to LiBH₄.⁵⁵) The energetics of each reaction are decomposed into a sequence having increasingly more physical contributions to the reaction thermodynamics, $\Delta E \rightarrow \Delta H^{T=0K} \rightarrow \Delta H^{T=300K} \rightarrow \Delta G^{T=300K}$, which allows us to gauge the importance of these contributions in comparison to the common practice of evaluating only static zero-Kelvin energetics. [ΔE refers to differences in the static zero-Kelvin energies (E in Eq. 3), and $\Delta H^{T=0K}$ adds ZPE contributions to ΔE .] Both formation reactions in Table VI are predicted to be exothermic ($\Delta H < 0$), in agreement with reports of spontaneous Li₄BN₃H₁₀ formation from the literature.^{4,7,12} As expected, formation from the elements vs. from the hydride mixture is a substantially more exothermic process.

It is noteworthy that dynamical contributions to the reaction energies are significant in reaction (a) ($\Delta E \neq \Delta H$), but appear to play a minor role in reaction (b) ($\Delta E \approx \Delta H$). By examining the values presented in Table IV for the phases participating in reaction (b) (Li₄BN₃H₁₀, LiNH₂, & LiBH₄) we see that these terms are sizable, but that they largely cancel out. This cancellation effect can be understood by the similarities in internal bonding shared by these three phases: Li₄BN₃H₁₀, with its Li⁺, BH₄⁻, and NH₂⁻ ions is essentially an amalgam

of the structures present in LiNH₂ and LiBH₄.

Turning now to the dehydrogenation of Li₄BN₃H₁₀, we note first that although several dehydrogenation products have been observed in experimental studies,^{4,5,7,8} the precise identity and respective proportions of these phases have not yet been definitively determined.^{4,7} For example, Aoki *et al.* reported unidentified diffraction peaks after dehydrogenation at $2\theta = 25^\circ$ and 35° . A technique for predicting possible decomposition pathways would be of significant value in helping to understand these reactions. However, decomposition pathways and products are difficult to predict *a priori*. To this end, we have scanned through the thermodynamics of a large number of candidate dehydrogenation reactions over a wide temperature range in order to identify the energetically favored products.⁵⁵

Calculated thermodynamics for seventeen candidate Li₄BN₃H₁₀ dehydrogenation reactions are listed in Table VII. In addition to the room-temperature energetics, there we also present data for $T = 460$ K, which is slightly below the melting point of pure Li₄BN₃H₁₀. Unlike the Li₄BN₃H₁₀ formation reaction, which can proceed at room temperature,⁴ dehydrogenation of Li₄BN₃H₁₀ has been reported only at elevated temperatures. In the case of pure Li₄BN₃H₁₀, dehydrogenation occurs above ~ 520 K, about 60 degrees above the melting temperature.⁴ However, a significant reduction in dehydrogenation temperature was observed upon the addition of a small amount of a Pt/Vulcan carbon catalyst.⁶ In this latter case hydrogen release occurred from the solid phase at $T > 390$ K. To more completely assess the dehydrogenation thermodynamics over a range of relevant temperatures, in Fig. 2 we plot the enthalpies and free energies of the candidate reactions for $T = 0$ –1000 K.

Out of the seventeen reactions considered, three reactions—(i), (c), and (f)—emerge as the most-favorable reactions in distinct temperature regimes (see Fig. 2, bottom panel). For low temperatures reaction (i) is preferred, followed at increasing temperatures by reaction (c) and reaction (f). More specifically, the favored products and their respective temperature ranges of stability are:

$$\begin{aligned}
 0 \text{ K} \leq T \leq 300 \text{ K}: & \quad 2\text{LiNH}_2 + 2\text{LiH} + \text{BN} + 2\text{H}_2 \\
 300 \text{ K} \leq T \leq 700 \text{ K}: & \quad \text{Li}_3\text{BN}_2 + \text{LiNH}_2 + 4\text{H}_2 \\
 700 \text{ K} \leq T: & \quad \text{Li}_3\text{BN}_2 + \text{LiH} + \frac{1}{2}\text{N}_2 + \frac{9}{2}\text{H}_2
 \end{aligned}$$

The relatively large entropy of the gas phase products plays an important role in determining which reaction is favored at a given temperature. Reactions yielding greater quantities of gaseous products should be favored with increasing T , and this is consistent with the observed trend: reaction (i), 2 mols \rightarrow reaction (c), 4 mols \rightarrow reaction (f), 5 mols. (It should be noted that at high temperatures—and certainly above the melting point of Li₄BN₃H₁₀—the harmonic approximation will no longer be valid, so we expect some decrease in accuracy with increasing T .)

Of the three favorable dehydrogenation reactions, only reaction (c), Li₄BN₃H₁₀ \rightarrow Li₃BN₂ + LiNH₂ + 4H₂, takes place within the temperature range where H₂-desorption (from undoped Li₄BN₃H₁₀) has been experimentally observed ($T \sim 520$ –630 K). While our prediction of Li₃BN₂ as a dehydrogenation product is consistent with experimental observa-

TABLE VI: Formation energies of $\text{Li}_4\text{BN}_3\text{H}_{10}$ [in kJ/(mol $\text{Li}_4\text{BN}_3\text{H}_{10}$)]. ΔE corresponds to the static zero Kelvin DFT energies; $\Delta H^{T=0\text{K}}$ adds the zero point energies to ΔE ; $\Delta H^{T=300\text{K}}$ (Eq. 3) adds finite-temperature vibrational (and molecular rotational+translational+ pV) energies to $\Delta H^{T=0\text{K}}$; $\Delta G^{T=300\text{K}}$ (Eq. 4) includes all of the contributions to $\Delta H^{T=300\text{K}}$ and adds vibrational (solids) or tabulated (molecular) entropies.

Rxn. No.	Reaction	ΔE	$\Delta H^{T=0\text{K}}$	$\Delta H^{T=300\text{K}}$	$\Delta G^{T=300\text{K}}$
(a)	$4 \text{Li} + \text{B} + \frac{3}{2}\text{N}_2 + 5\text{H}_2 \rightarrow \text{Li}_4\text{BN}_3\text{H}_{10}$	-806.9	-670.2	-708.1	-454.6
(b)	$3 \text{LiNH}_2 + \text{LiBH}_4 \rightarrow \text{Li}_4\text{BN}_3\text{H}_{10}$	-11.3	-11.2	-11.8	-10.2

TABLE VII: Calculated reaction energies [ΔE in kJ/(mol H_2)], enthalpies [ΔH in kJ/(mol H_2)], and free energies [ΔG in kJ/mol products] for candidate $\text{Li}_4\text{BN}_3\text{H}_{10}$ dehydrogenation reactions.

Rxn. No.	Reaction	ΔE	$\Delta H^{T=0\text{K}}$	$\Delta H^{T=300\text{K}}$	$\Delta H^{T=460\text{K}}$	$\Delta G^{T=300\text{K}}$	$\Delta G^{T=460\text{K}}$
(c)	$\text{Li}_4\text{BN}_3\text{H}_{10} \rightarrow \text{Li}_3\text{BN}_2 + \text{LiNH}_2 + 4\text{H}_2$	28.2	5.7	11.2	12.5	-88.8	-161.3
(d)	$\text{Li}_4\text{BN}_3\text{H}_{10} \rightarrow \text{Li}_3\text{BN}_2 + \frac{1}{2}\text{Li}_2\text{NH} + \frac{1}{2}\text{NH}_3 + 4\text{H}_2$	40.6	17.7	23.4	24.3	-61.4	-145.2
(e)	$\text{Li}_4\text{BN}_3\text{H}_{10} \rightarrow \text{Li}_3\text{BN}_2 + \text{LiH} + \text{NH}_3 + 3\text{H}_2$	42.6	17.5	23.5	24.0	-71.6	-148.0
(f)	$\text{Li}_4\text{BN}_3\text{H}_{10} \rightarrow \text{Li}_3\text{BN}_2 + \text{LiH} + \frac{1}{2}\text{N}_2 + \frac{9}{2}\text{H}_2$	50.2	24.1	29.7	30.8	-38.2	-131.0
(g)	$\text{Li}_4\text{BN}_3\text{H}_{10} \rightarrow \text{Li}_3\text{BN}_2 + \text{Li} + \frac{1}{2}\text{N}_2 + 5\text{H}_2$	61.9	37.4	43.5	44.6	23.0	-82.2
(h)	$\text{Li}_4\text{BN}_3\text{H}_{10} \rightarrow \text{Li}_3\text{BN}_2 + \text{Li} + \text{NH}_3 + \frac{7}{2}\text{H}_2$	60.4	37.5	44.1	44.7	-10.5	-99.2
(i)	$\text{Li}_4\text{BN}_3\text{H}_{10} \rightarrow 2\text{LiNH}_2 + 2\text{LiH} + \text{BN} + 2\text{H}_2$	6.4	-19.4	-16.1	-15.4	-90.1	-121.2
(j)	$\text{Li}_4\text{BN}_3\text{H}_{10} \rightarrow \text{LiNH}_2 + \text{Li}_3\text{N} + \text{BN} + 4\text{H}_2$	56.9	35.8	40.5	41.3	34.1	-34.9
(k)	$\text{Li}_4\text{BN}_3\text{H}_{10} \rightarrow 4\text{LiH} + \text{BN} + \text{N}_2 + 3\text{H}_2$	79.6	44.1	48.5	48.8	11.1	-60.7
(l)	$\text{Li}_4\text{BN}_3\text{H}_{10} \rightarrow 2\text{Li}_2\text{NH} + \text{BN} + 4\text{H}_2$	45.3	23.3	27.9	28.8	-14.9	-83.3
(m)	$\text{Li}_4\text{BN}_3\text{H}_{10} \rightarrow 2\text{LiNH}_2 + \text{BN} + 2\text{Li} + 3\text{H}_2$	60.0	39.5	45.1	46.2	32.3	-23.6
(n)	$\text{Li}_4\text{BN}_3\text{H}_{10} \rightarrow \text{LiNH}_2 + \text{Li}_2\text{NH} + \text{LiH} + \text{BN} + 3\text{H}_2$	32.3	9.1	13.2	14.1	-52.5	-102.3
(o)	$\text{Li}_4\text{BN}_3\text{H}_{10} \rightarrow \text{Li}_2\text{NH} + 2\text{LiH} + \text{BN} + \text{NH}_3 + 2\text{H}_2$	55.9	28.5	32.7	32.1	-35.4	-88.9
(p)	$\text{Li}_4\text{BN}_3\text{H}_{10} \rightarrow \text{LiNH}_2 + 3\text{LiH} + \text{BN} + \text{NH}_3 + \text{H}_2$	27.7	-9.1	-6.6	-8.8	-73.0	-107.9
(q)	$\text{Li}_4\text{BN}_3\text{H}_{10} \rightarrow \text{Li}_3\text{N} + \text{LiH} + \text{BN} + \text{NH}_3 + 3\text{H}_2$	80.9	57.7	62.6	62.4	51.3	-21.6
(r)	$\text{Li}_4\text{BN}_3\text{H}_{10} \rightarrow \frac{1}{2}\text{Li}_2\text{NH} + \text{Li}_3\text{N} + \text{BN} + \frac{1}{2}\text{NH}_3 + 4\text{H}_2$	69.3	47.8	52.7	53.2	61.5	-18.8
(s)	$\text{Li}_4\text{BN}_3\text{H}_{10} \rightarrow \text{Li}_3\text{BN}_2 + \frac{1}{3}\text{Li}_3\text{N} + \frac{2}{3}\text{NH}_3 + 4\text{H}_2$	48.7	26.0	31.7	32.5	-35.9	-123.6

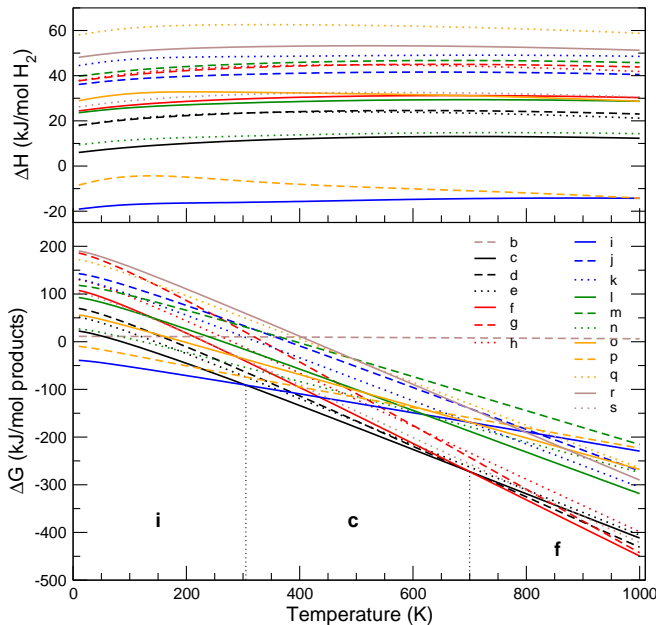


FIG. 2: (Color online) Calculated enthalpies (ΔH , top panel) and free energies (ΔG , bottom panel) of candidate $\text{Li}_4\text{BN}_3\text{H}_{10}$ dehydrogenation reactions as a function of temperature at $p = 1$ bar. The reactions are labeled as in Table VII.

tions, we are not aware of any reports indicating the presence of LiNH_2 . This discrepancy is likely due to the fact that most experiments have been performed on off-stoichiometric $\text{Li}_4\text{BN}_3\text{H}_{10}$ formed from 2:1 LiNH_2 : LiBH_4 mixtures. Mixtures with this composition are deficient in the Li and N presumably needed to yield the additional amide present in our calculations.

The calculated enthalpy for reaction (c) ranges from 11.2 to 12.8 kJ/(mol H_2) for $T = 300$ – 500 K, indicating that H_2 release is a weakly endothermic process. For the higher-temperature reaction (f), dehydrogenation is likewise predicted to be endothermic with a slightly larger enthalpy of ~ 31 kJ/(mol H_2). Only the low temperature reaction (i) with $\Delta H \approx -(16$ – $19)$ kJ/(mol H_2) is found to be exothermic. It would be interesting to test whether the predicted temperature-dependent decomposition sequence [(i) \rightarrow (c) \rightarrow (f)] could be observed experimentally by holding $\text{Li}_4\text{BN}_3\text{H}_{10}$ at temperatures within each of the reaction regimes for long times.

Based on the data presented in Fig. 2 and Table VII, H_2 desorption from $\text{Li}_4\text{BN}_3\text{H}_{10}$ is thermodynamically favorable at essentially all non-zero temperatures: the negative free energies of dehydrogenation suggest that $\text{Li}_4\text{BN}_3\text{H}_{10}$ is metastable with respect to decomposition via one of the reactions (i), (c), or (f). On the other hand, experiments⁴ on pure $\text{Li}_4\text{BN}_3\text{H}_{10}$ indicate that desorption does not take place until the tempera-

ture is raised above 520 K. Taken together, these factors suggest that the relatively high temperatures needed in practice for H₂-release are a consequence of poor kinetics, not unfavorable thermodynamics.

An important distinction between our calculations and the experimental dehydrogenation of undoped Li₄BN₃H₁₀ concerns the phase of Li₄BN₃H₁₀ present during the dehydrogenation reaction. As mentioned above, pure Li₄BN₃H₁₀ releases hydrogen from the molten state.⁴ Similarly, H₂ release from other hydride phases, such as LiBH₄, also occurs from the molten state.⁴⁸ Due to the computational expense associated with obtaining precise energetics for liquids using DFT, this study, and previous studies on LiBH₄,^{41,48} have modeled the dehydrogenation reaction as a solid-state reaction. Since the enthalpy of the liquid phase will be more positive than that of the corresponding solid phase, the calculated solid-state enthalpy of reaction (c) evaluated at the melting point (T_{mp}), $\Delta H^{T_{\text{mp}}} = 12.5$ kJ/(mol H₂), represents an *upper bound* on the enthalpy for desorption from liquid Li₄BN₃H₁₀. It will be possible to more precisely estimate the magnitude by which ΔH is overestimated once the latent heat of melting for Li₄BN₃H₁₀ has been measured. Until such data become available, it nevertheless seems reasonable to conclude that the dehydrogenation of Li₄BN₃H₁₀ is either weakly endothermic, or exothermic. This conclusion is consistent with the failed attempts at re-hydriding Li₄BN₃H₁₀ reported thus far in the literature,⁴ as a small (positive) enthalpy of dehydrogenation will result in a similarly small thermodynamic driving force for re-hydriding. On the other hand, for Li₄BN₃H₁₀ doped with Pt/Vulcan carbon,⁶ dehydrogenation begins below T_{mp} . In this case our approach of modeling solid state reactions more accurately captures the true phase behavior of Li₄BN₃H₁₀, neglecting the possible formation of C- or Pt-containing compounds.

V. CONCLUSION

Density functional theory calculations have been employed to study the crystal structure and the finite-temperature formation and dehydrogenation thermodynamics of Li₄BN₃H₁₀. The calculations have resolved the discrepancies in hydrogen bond lengths between the separate structures determined via X-ray and neutron diffraction experiments, and suggest that the neutron data yields a slightly more accurate description of the crystal structure. All three of the reported experimental

crystal structures relax to essentially the same structure.

For reaction energetics, our calculations indicate that Li₄BN₃H₁₀ formation is exothermic, and that the dehydrogenation enthalpy of solid-state Li₄BN₃H₁₀ is temperature-dependent: H₂ release is exothermic at low temperatures, and weakly endothermic at the higher temperatures probed by recent experiments. A non-zero latent heat for Li₄BN₃H₁₀ melting will reduce the dehydrogenation enthalpy from the liquid state (relative to the solid state), but the size of this effect is still to be determined. To help clarify the identity of the phases produced via dehydrogenation we have performed a computational search over 17 candidate dehydrogenation reactions, and identified three reactions having favorable thermodynamics spanning the temperature range $T = 0$ –1000 K. All three of these reactions exhibit a decrease in free energy, suggesting that Li₄BN₃H₁₀ is a metastable phase. For temperatures where H₂-desorption has been experimentally observed, the thermodynamically-favored reaction is Li₄BN₃H₁₀ \rightarrow Li₃BN₂ + LiNH₂ + 4H₂, with an enthalpy of 11.2–12.8 kJ/(mol H₂). The relatively small dehydriding enthalpies are consistent with the failed re-hydriding attempts reported in the literature, and suggest that hydrogen release from Li₄BN₃H₁₀ is a kinetically—rather than thermodynamically—hindered process.

Note added in proof—During the review of this manuscript two new studies of Li₄BN₃H₁₀ were brought to our attention.^{49,50} In the first study Noritake and co-workers⁵⁰ performed a crystal structure analysis of Li₄BN₃H₁₀ using synchrotron X-ray diffraction. While they found external structural parameters (bcc, space group $I2_13$, $a = 10.67$ Å) consistent with the two reports cited previously,^{11,12} the reported N–H bond lengths were more consistent with the neutron data of Ref. 12 (and with our calculated N–H distances) than the X-ray data of Ref. 11. In the other recent study, Herbst and Hector⁴⁹ examined the electronic structure and energetics of Li₄BN₃H₁₀ using DFT. Our results appear to be consistent with their findings.

Acknowledgments

The authors thank D. Halliday, A. Sudik, and J. Yang for reviewing a preliminary version of this manuscript. V. Ozoliņš thanks the U.S. Department of Energy for financial support under grant DE-FG02-05ER46253.

¹ U. S. National Academy of Sciences, *The Hydrogen economy: Opportunities, Cost, Barriers and R&D Needs* (The National Academies Press, Washington, D.C., 2004).

² L. Schlapbach and A. Züttel, *Nature* **414**, 353 (2001).

³ *Targets for on-board hydrogen storage systems*, URL <http://www.eere.energy.gov/hydrogenandfuelcells/sr橙/orange-and-sr橙/blue-applications-2005-page.pdf>.

⁴ F. E. Pinkerton, G. P. Meisner, M. S. Meyer, M. P. Balogh, and M. D. Kundrat, *J. Phys. Chem. B Lett.* **109**, 6 (2005), see also supplementary information accompanying this article.

⁵ G. P. Meisner, M. L. Scullin, M. P. Balogh, F. E. Pinkerton, and M. S. Meyer, *J. Phys. Chem. B* **110**, 4186 (2006).

⁶ F. E. Pinkerton, M. S. Meyer, G. P. Meisner, and M. P. Balogh, *J. Phys. Chem. B* **110**, 7967 (2006).

⁷ M. Aoki, K. Miwa, T. Noritake, G. Kitahara, Y. Nakamori, S. Orimo, and S. Tawata, *Appl. Phys. Lett.* **89**, 1409 (2006).

⁸ Y. Nakamori, A. Ninomiya, G. Kitahara, M. Aoki, T. Noritake, K. Miwa, Y. Kojima, and S. Orimo, *J. Power Sources* **155**, 447 (2006).

- ⁹ B. Bogdanović and M. Schwickardi, *J. Alloys Compd.* **253-254**, 1 (1997).
- ¹⁰ A. Gutowska, L. Li, Y. Shin, C. M. Wang, X. S. Li, J. C. Linehan, R. S. Smith, B. D. Kay, B. Schmid, W. Shaw, et al., *Angew. Chem. Int. Ed.* **44**, 3578 (2005).
- ¹¹ Y. E. Filinchuk, K. Yvon, G. P. Meisner, F. E. Pinkerton, and M. P. Balogh, *Inorg. Chem.* **45**, 1433 (2006).
- ¹² P. A. Chater, W. I. F. David, S. R. Johnson, P. P. Edwards, and P. A. Anderson, *Chem. Commun.* **23**, 2439 (2006).
- ¹³ P. Hohenberg and W. Kohn, *Phys. Rev.* **136**, B864 (1964).
- ¹⁴ W. Kohn and L. J. Sham, *Phys. Rev.* **140**, A1133 (1965).
- ¹⁵ J. P. Perdew, J. A. Chevary, S. H. Vosko, et al., *Phys. Rev. B* **46**, 6671 (1992).
- ¹⁶ G. Kresse and J. Furthmüller, *Phys. Rev. B* **54**, 11169 (1996).
- ¹⁷ P. E. Blöchl, *Phys. Rev. B* **50**, 17953 (1994).
- ¹⁸ G. Kresse and D. Joubert, *Phys. Rev. B* **59**, 1758 (1999).
- ¹⁹ H. J. Monkhorst and J. D. Pack, *Phys. Rev. B* **13**, 5188 (1976).
- ²⁰ D. C. Wallace, *Thermodynamics of Crystals* (John Wiley & Sons, 1972).
- ²¹ J. M. Rickman and R. LeSar, *Annu. Rev. Mater. Res.* **32**, 195 (2002).
- ²² S. Wei and M. Y. Chou, *Phys. Rev. Lett.* **69**, 2799 (1992).
- ²³ M. W. Chase, Jr., *NIST-JANAF Thermochemical Tables, 4th Edition* (American Chemical Society, 1998).
- ²⁴ D. R. Lide, ed., *CRC Handbook of Chemistry and Physics* (Taylor and Francis, 2005), 86th ed.
- ²⁵ A. C. Switendick and B. Morosin, *American Institute of Physics: Conf. Proc.* **231**, 205 (1991).
- ²⁶ R. H. Wentorf, Jr., *J. Chem. Phys.* **26**, 956 (1957).
- ²⁷ P. Villars and L. D. Calvert, eds., *Pearson's Handbook of Crystallographic Data for Intermetallic Phases*, vol. 2,4 (ASM International, Materials Park, OH, 1991), 2nd ed.
- ²⁸ J. P. Vidal and G. Vidal-Valat, *Acta Crystallographica B* **42**, 131 (1986).
- ²⁹ H. Jacobs and R. Juza, *Zeitschrift fuer Anorganische und Allgemeine Chemie* **391**, 271 (1972).
- ³⁰ K. Cenzual, L. M. Gelato, M. Penzo, and E. Parthe, *Acta Crystallographica B* **47**, 433 (1991).
- ³¹ H. Yamane, S. Kikkawa, and M. Koizumi, *J. Solid State Chem.* **71**, 1 (1987).
- ³² H. Yamane, S. Kikkawa, H. Horiuchi, and M. Koizumi, *J. Solid State Chem.* **65**, 6 (1986).
- ³³ F. E. Pinkerton and J. F. Herbst, *J. Appl. Phys.* **99**, 113523 (2006).
- ³⁴ J.-P. Soulie, G. Renaudin, R. Cerny, and K. Yvon, *J. Alloys Compd.* **346**, 200 (2002).
- ³⁵ K. Miwa, N. Ohba, S. Towata, Y. Nakamori, and S. Orimo, *Phys. Rev. B* **71**, 195109 (2005).
- ³⁶ B. Magyari-Köpe, V. Ozoliņš, and C. Wolverton, *Phys. Rev. B* **73**, 220101 (2006).
- ³⁷ R. H. Jr., Wentorf, *J. Phys. Chem.* **34**, 809 (1961).
- ³⁸ R. C. DeVries and J. F. Fleischer, *Mat. Res. Bull.* **4**, 433 (1969).
- ³⁹ D. J. Siegel, to be published.
- ⁴⁰ T. J. Frankcombe and G.-J. Kroes, *Phys. Rev. B* **73**, 174302 (2006).
- ⁴¹ K. Miwa, N. Ohba, and S. Towata, *Phys. Rev. B* **69**, 245120 (2004).
- ⁴² J. F. Herbst and L. G. Hector, Jr., *Phys. Rev. B* **72**, 125120 (2005).
- ⁴³ J. E. Northrup, R. D. Flice, and J. Neugebauer, *Phys. Rev. B* **56**, R4325 (1997).
- ⁴⁴ G. Kern, G. Kresse, and J. Hafner, *Phys. Rev. B* **59**, 8551 (1999).
- ⁴⁵ Z. Łodziana and T. Vegge, *Phys. Rev. Lett.* **93**, 145501 (2004).
- ⁴⁶ P. Chen, Z. Xiong, J. Luo, J. Lin, and K. L. Tan, *Nature (London)* **420**, 302 (2002).
- ⁴⁷ L. A. Curtiss, K. Raghavachari, P. C. Redfern., and J. A. Pople, *J. Chem. Phys.* **106**, 1063 (1997).
- ⁴⁸ T. J. Frankcombe, G.-J. Kroes, and A. Züttel, *Chem. Phys. Lett.* **405**, 73 (2005).
- ⁴⁹ J. F. Herbst and L. G. Hector, Jr., *Appl. Phys. Lett.* **88**, 231904 (2006).
- ⁵⁰ T. Noritake, M. Aoki, S. Towata, A. Ninomiya, Y. Nakamori, and S. Orimo, *Appl. Phys. A* **83**, 277 (2006).
- ⁵¹ More specifically, the potentials employed for evaluating zero-Kelvin energies and geometries were (in the parlance of the VASP database): Li_sv, B_h, N_h, and H_h, with respective valence electron configurations of $1s^2 2s^1$, $2s^2 2p^1$, $2s^2 2p^3$, and $1s^1$.
- ⁵² The geometry of each structure was re-optimized using the softer PAW set before the dynamical matrix calculations were performed.
- ⁵³ Our somewhat non-standard approach of using softer potentials to determine the vibrational spectra of the solid phases, but hard (semi-core) potentials for the remaining properties (zero-Kelvin energetics, ground state geometries, and molecular vibrational spectra,) is based on three considerations: First, the softer PAW set allows for more efficient calculations with a reduced planewave cutoff energy, thus permitting larger supercells and, consequently, smaller finite-size effects in the phonon spectrum. Second, our calculated formation energies for LiH, LiNH₂, and Li₂NH at $T = 300$ K agree with the hard PAW results in Ref. 42 to within 1 kJ/mol f.u. Third, testing revealed that the hard potentials yielded molecular vibrational frequencies which were in slightly better agreement with experimental data than those obtained with the softer PAW set. For example, for N₂, where the differences between calculated vibrational frequencies are largest, we find 2338 (2452) cm⁻¹ from the hard (soft) PAW sets, compared with an experimental value of 2359 cm⁻¹.²⁴ However, this slight discrepancy in frequencies has only a small impact on vibrational thermodynamic properties—for example, ZPEs calculated with both PAW sets differ by 0.7 kJ/mol f.u. at most. It therefore seems likely that an approach where *all* vibrational properties (solids and molecules) were evaluated using the softer potentials would also yield reasonably precise results. We thus conclude that our approach of mixing potentials gives results comparable in precision to those obtained with the hard PAW set alone, but without the associated computational expense.
- ⁵⁴ The discrepancy in calculated vs. experimental enthalpy for Li₂NH has been noted in Ref. 42, and it has been suggested that the experimental measurement be revisited in light of the good agreement for the other Li-containing compounds: LiH, LiNH₂, and LiBH₄. To our knowledge the formation enthalpy of Li₂NH reported in Ref. 46 has not been independently confirmed.
- ⁵⁵ Due to the computational difficulty associated with treating a non-stoichiometric phase, our calculations are restricted to the stoichiometric composition “Li₄BN₃H₁₀,” whereas most experiments have focused on 2:1 LiNH₂:LiBH₄ off-stoichiometric “Li₃BN₂H₈” mixtures, which have been found to minimize⁵ NH₃ release.